Extraordinarily high spectral sensitivity in refractive index sensors using multiple optical modes

Zongfu Yu* and Shanhui Fan

Ginzton Lab, Department of Electrical Engineering, Stanford University, Stanford, CA, 94305 USA
*zfyu@stanford.edu

Abstract: The extraordinary spectral sensitivity of surface plasmon resonance (SPR) sensors is commonly attributed to the modal overlap or unique dispersion of surface plasmons. In contrast to this belief, we show that such high sensitivity is due to the multi-mode nature of the sensing scheme. This concept of multi-mode sensing can be applied to dielectric systems as well in order to achieve similar extraordinary spectral sensitivity. We also show that there is a fundamental constraint between the spectral sensitivity and quality factor in such multi-mode sensing approach.

©2011 Optical Society of America

OCIS codes: (130.6010) Sensors; (240.6680) Surface plasmons; (230.5750) Resonators.

References and links

1. W. Lukosz, "Principles and sensitivities of integrated optical and surface plasmon sensors for direct affinity sensing and immunosensing," Biosens. Bioelectron. **6**(3), 215–225 (1991).
2. B. Johnsson, S. Löfås, and G. Lindquist, "Immobilization of proteins to a carboxymethyldextran-modified gold surface for biospecific interaction analysis in surface plasmon resonance sensors," Anal. Biochem. **198**(2), 268–277 (1991).
3. M. A. Cooper, "Optical biosensors in drug discovery," Nat. Rev. Drug Discov. **1**(7), 515–528 (2002).
4. V. S.-Y. Lin, K. Motesharei, K.-P. S. Dancil, M. J. Sailor, and M. R. Ghadiri, "A porous silicon-based optical interferometric biosensor," Science **278**(5339), 840–843 (1997).
5. B. Liedberg, C. Nylander, and I. Lundström, "Biosensing with surface plasmon resonance--how it all started," Biosens. Bioelectron. **10**(8), i–ix (1995).
6. R. Cush, J. M. Cronin, W. J. Stewart, C. H. Maule, J. Molloy, and N. J. Goddard, "The resonant mirror: a novel optical biosensor for direct sensing of biomolecular interactions part I: principle of operation and associated instrumentation," Biosens. Bioelectron. **8**(7-8), 347–354 (1993).
7. A. J. Haes, and R. P. Van Duyne, "A nanoscale optical biosensor: sensitivity and selectivity of an approach based on the localized surface plasmon resonance spectroscopy of triangular silver nanoparticles," J. Am. Chem. Soc. **124**(35), 10596–10604 (2002).
8. C. L. Baird, and D. G. Myszka, "Current and emerging commercial optical biosensors," J. Mol. Recognit. **14**(5), 261–268 (2001).
9. J. Homola, "On the sensitivity of surface plasmon resonance sensors with spectral interrogation," Sens. Actuators B Chem. **41**(1-3), 207–211 (1997).
10. J. Homola, S. S. Yee, and G. Gauglitz, "Surface plasmon resonance sensors: review," Sens. Actuators B Chem. **54**(1-2), 3–15 (1999).
11. S. Lal, S. Link, and N. J. Halas, "Nano-optics from sensing to waveguiding," Nat. Photonics **1**(11), 641–648 (2007).
12. G. G. Nenninger, P. Tobiska, J. Homola, and S. S. Yee, "Long-range surface plasmons for high-resolution surface plasmon resonance sensors," Sens. Actuators B Chem. **74**(1-3), 145–151 (2001).
13. B. Liedberg, C. Nylander, and I. Lunström, "Surface plasmon resonance for gas detection and biosensing," Sens. Actuators **4**, 299–304 (1983).
14. B. Cunningham, P. Li, B. Lin, and J. Pepper, "Colorimetric resonant reflection as a direct biochemical assay technique," Sens. Actuators B Chem. **81**(2-3), 316–328 (2002).
15. N. M. Hanumegowda, C. J. Stica, B. C. Patel, I. White, and X. Fan, "Refractometric sensors based on microsphere resonators," Appl. Phys. Lett. **87**(20), 201107 (2005).
16. A. Artar, A. A. Yanik, and H. Altug, "Fabry–Perot nanocavities in multilayered plasmonic crystals for enhanced biosensing," Appl. Phys. Lett. **95**(5), 051105 (2009).
17. W. Liang, Y. Huang, Y. Xu, R. K. Lee, and A. Yariv, "Highly sensitive fiber Bragg grating refractive index sensors," Appl. Phys. Lett. **86**(15), 151122 (2005).
18. M. Lončar, A. Scherer, and Y. Qiu, "Photonic crystal laser sources for chemical detection," Appl. Phys. Lett. **82**(26), 4648–4650 (2003).

19. E. Chow, A. Grot, L. W. Mirkarimi, M. Sigalas, and G. Girolami, "Ultracompact biochemical sensor built with two-dimensional photonic crystal microcavity," Opt. Lett. **29**(10), 1093–1095 (2004).
20. M. El Beheiry, V. Liu, S. Fan, and O. Levi, "Sensitivity enhancement in photonic crystal slab biosensors," Opt. Express **18**(22), 22702–22714 (2010).
21. A. Yalcin, K. C. Popat, J. C. Aldridge, T. A. Desai, J. Hryniewicz, N. Chbouki, B. E. Little, K. Oliver, V. Van, C. Sai, D. Gill, M. Anthes-Washburn, M. S. Unlu, and B. B. Goldberg, "Optical sensing of biomolecules using microring resonators," IEEE J. Sel. Top. Quantum Electronics **12**(1), 148–155 (2006).
22. J. Zhu, S. K. Ozdemir, Y.-F. Xiao, L. Li, L. He, D.-R. Chen, and L. Yang, "On-chip single nanoparticle detection and sizing by mode splitting in an ultrahigh-Q microresonator," Nat. Photonics **4**(1), 46–49 (2010).
23. C. Chung-Yen, W. Fung, and L. J. Guo, "Polymer microring resonators for biochemical sensing applications," IEEE J. Sel. Top. Quant. Electron. **12**(1), 134–142 (2006).
24. J. N. Anker, W. P. Hall, O. Lyandres, N. C. Shah, J. Zhao, and R. P. Van Duyne, "Biosensing with plasmonic nanosensors," Nat. Mater. **7**(6), 442–453 (2008).
25. J. J. Mock, D. R. Smith, and S. Schultz, "Local refractive index dependence of plasmon resonance spectra from individual nanoparticles," Nano Lett. **3**(4), 485–491 (2003).
26. H. Xu, and M. Käll, "Modeling the optical response of nanoparticle-based surface plasmon resonance sensors," Sens. Actuators B Chem. **87**(2), 244–249 (2002).
27. I. M. White, and X. Fan, "On the performance quantification of resonant refractive index sensors," Opt. Express **16**(2), 1020–1028 (2008).
28. A. V. Kabashin, P. Evans, S. Pastkovsky, W. Hendren, G. A. Wurtz, R. Atkinson, R. Pollard, V. A. Podolskiy, and A. V. Zayats, "Plasmonic nanorod metamaterials for biosensing," Nat. Mater. **8**(11), 867–871 (2009).
29. J. Hu, X. Sun, A. Agarwal, and L. C. Kimerling, "Design guidelines for optical resonator biochemical sensors," J. Opt. Soc. Am. B **26**(5), 1032–1041 (2009).
30. X. Fan, I. M. White, S. I. Shopova, H. Zhu, J. D. Suter, and Y. Sun, "Sensitive optical biosensors for unlabeled targets: a review," Anal. Chim. Acta **620**(1-2), 8–26 (2008).
31. J. D. Joannopoulos, S. G. Johnson, J. N. Winn, and R. D. Meade, *Photonic Crystals: Modeling the Flow of Light,* 2 ed. pp.18 (Princeton University Press, Princeton, New Jersey, 2008).
32. A. Raman, and S. Fan, "Perturbation theory for plasmonic modulation and sensing," under review (2010).
33. P. B. Johnson, and R. W. Christy, "Optical constants of the noble metals," Phys. Rev. B **6**(12), 4370–4379 (1972).

1. Introduction

Refractive index sensing has a wide range of applications in areas such as life science [1–8]. One of the most widely used approaches involves detecting the spectral shift of a resonant feature as the refractive index is varied [9]. A prominent example of such refractive index sensor is the surface plasmon resonance (SPR) sensor [9–13], which has been commercialized [8]. A typical SPR sensor consists of a dielectric prism with a thin-layer of metal coating on its top (Fig. 1a). As a result of surface plasmon excitation, the reflection spectrum for light propagating through the prism exhibits a dip. Such a dip will shift in wavelength when the refractive index changes at the surface of the metal (Fig. 1b).
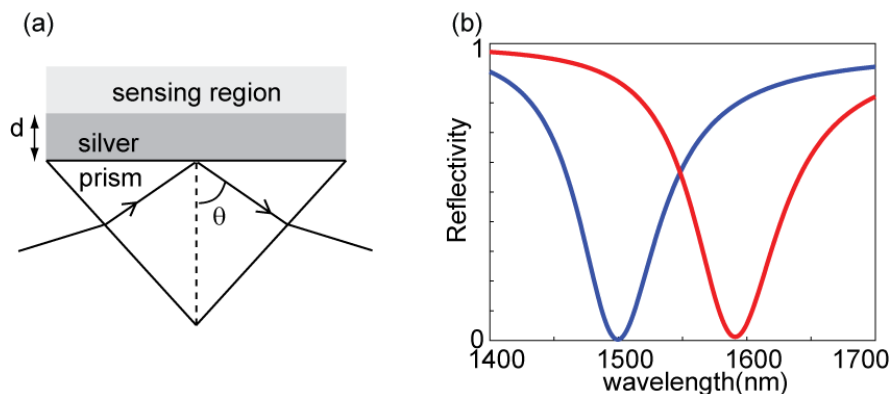

Fig. 1. (a) Schematic of a surface plasmon resonance sensor. (b) Reflectivity spectra when the index perturbation $\Delta n = 0.001$ is absent (blue) and present (red). The index change is applied to the sensing region (assumed to be air) above the silver film.

Another example of resonant refractive index sensors is the resonant cavity index sensor [14–17], a simplest configuration of which is shown in Fig. 2a. The sensor consists of a

Fabry-Perot cavity (Fig. 2a) exhibiting a resonant peak in its transmission spectrum. The resonant peak shifts when the refractive index of the material in the cavity changes (Fig. 2b).
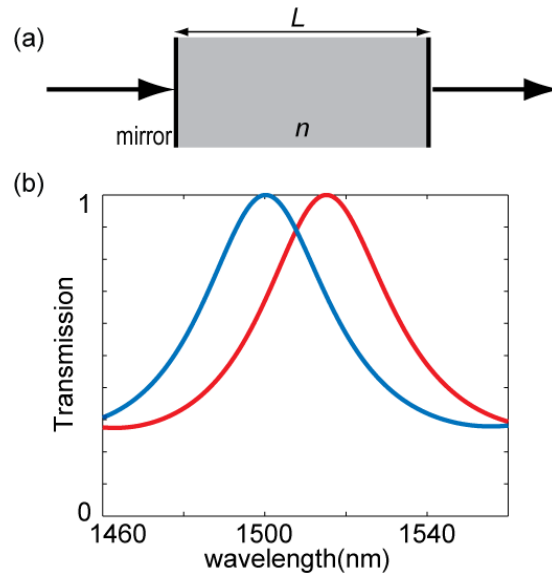

Fig. 2. (a) Schematic of a Fabry-Perot cavity senor. (b) Transmission spectra when the index perturbation $\Delta n = 0.035$ is absent (blue) and present (red).The index change is applied to the whole cavity excluding the mirrors.

In both of the examples above, a shift in the resonant wavelength $\Delta\lambda$ provides information about the refractive index shift Δn. Thus, it is standard to define the *spectral sensitivity* of such sensors as $S = \Delta\lambda / \Delta n$. The spectral sensitivity has a unit of nm/RIU, where RIU is the refractive index unit. The resonant cavity scheme (Fig. 2a) in general has a spectral sensitivity on the order of 10^2-10^3 nm/RIU in the optical wavelength range. This holds true for many different cavity types including photonic crystal resonators [14, 18–20], micro-cavity resonators [15, 21–23], and localized surface plasmon resonators [7, 24–26]. On the other hand, in the similar wavelength range, the spectral sensitivity of SPR is well above 10^4 nm/RIU [27,28]. Even though such a large difference in spectral sensitivity is well known, the physical mechanism that underlies such a difference, to the best of our knowledge, has never been explicitly pointed out. Instead, it was typically implied that the large sensitivity is a unique nature of surface plasmon polariton [6].

In this paper, we provide a general unified picture on the issue of spectral sensitivity in resonance-based refractive index sensing schemes. We show that for a system involving only a single resonance mode, its spectral sensitivity cannot exceed λ / n, which for an infrared or visible light translates to a maximum sensitivity of $10^2 - 10^3$ nm/RIU. We also show that the extraordinarily large spectral sensitivity of a SPR sensor is due entirely to a multi-mode nature of the SPR system. The SPR system supports a continuum of modes, each with a different wavevector. As the index shifts, the system is probing different modes with different wavevectors. Based on this understanding, we design dielectric-based structures that have comparable spectral sensitivity as SPR sensors, and thus demonstrate that the extraordinary large sensitivity is not unique to the plasmonic system.

To compare the ultimate performance of different sensors, one in fact needs to compare the *detection limit* [27, 29], which measures the smallest refractive index shift that is detectable. It is known that the spectral sensitivity itself does not determine the detection limit. The SPR sensor systems, while having a large spectral sensitivity, also have a low quality factor Q, whereas dielectric resonant systems typically have lower spectral sensitivity, but higher Q. As a result, in spite of the large difference in spectral sensitivity, the detection

limit of optimized sensors of both types is in fact comparable [30]. Here, we show that there is in fact an intrinsic tradeoff between spectral sensitivity and linewidth. As a result of this tradeoff, achieving a high detection limit ultimately will require systems with low intrinsic loss, which favors dielectric systems in general. We also show that for a given sensor system, one can exploit this tradeoff to achieve similar detection limit, while operating the system with a wider linewidth and a higher spectral sensitivity, and hence alleviating some of the difficulties in terms of stabilities associated with high-Q dielectric systems.

The paper is organized as follows: in Section 2, we describe the limit of sensitivity in schemes that use a single resonant mode. In Section 3, we reconfirm that the SPR sensor has an extraordinary spectral sensitivity far beyond such single-mode limit, and provide an analysis that relates the origin of the extraordinary sensitivity in SPR sensor to the multi-mode nature of the system. Then, building upon this analysis in Section 3, we show in Section 4 that a dielectric system can be designed to have similar extraordinary sensitivity and much higher quality factor. In Section 5, we provide a general discussion between the trade-off of quality factor and spectral sensitivity in this class of multi-mode sensor structures.

2. The single-mode limit for refractive-index sensing

We start by considering sensors that employ a single-mode resonant cavity as shown in Fig. 2a. As a concrete example, Fig. 2a illustrates a cavity structure consisting of a dielectric medium (with a refractive index n=3.5) sandwiched in between two high-reflectivity mirrors. By choosing the cavity length to be 3000nm, the cavity exhibits a Fabry-Perot resonance with a 100% transmission at the wavelength of $\lambda = 1500 nm$ (Fig. 2b, blue line). Increasing the refractive index of the medium by $\Delta n = 0.035$ results in a resonant wavelength shift of $\Delta\lambda = 15$ nm (Fig. 2a, red line). Thus, the spectral sensitivity of such a cavity sensor is $S = 429$ nm/RIU.

The resonance shift caused by refractive index change can be theoretically calculated using the perturbation theory as [31]:

$$\Delta\omega = -\frac{\omega}{2}\frac{\int d^3r \cdot \Delta\varepsilon(r)|E(r)|^2}{\int d^3r \cdot \varepsilon(r)|E(r)|^2}$$

(1)

where $E(r)$ is the electric field of the optical resonance; $\varepsilon(r)$ is the distribution of dielectric constant of the medium and ω is the resonant frequency. For a small change in the dielectric constant $\Delta\varepsilon \approx \varepsilon 2\Delta n / n$, using Eq. (1), we then obtain:

$$\frac{\Delta\lambda}{\lambda} = \frac{\Delta\omega}{\omega} \approx \frac{\Delta n}{n}$$

(2)

Here we assume that the index perturbation $\Delta\varepsilon(r)$ is applied to the entire structure. When the index perturbation occurs only in part of the dielectric structure, the fractional wavelength shift is smaller than $\Delta n / n$. In addition, material dispersion, resulting from having part of the modal energy stored in electronic motions [32], also reduces the fractional wavelength shift. Thus, Eq. (2) in fact sets an upper bound on the spectral sensitivity

$$S \leq \frac{\lambda}{n}$$

(3)

As an example, for a medium with refractive index 1.5 operating at 1500nm wavelength, this limit corresponds to a maximum sensitivity of about 1000 nm/RIU.

One can also define a normalized sensitivity

$$S_N = \frac{d\lambda / \lambda}{dn / n}$$

(4)

Equation (2) then shows that the maximum normalized sensitivity of single-resonance sensing is 1. It can be easily verified that the dielectric Fabry-Perot sensor shown in Fig. 2a in fact achieve the maximum normalized sensitivity $S_N = 1$, due to the perfect overlap between the refractive index perturbation and the resonant mode. The limit of Eq. (3) applies to most sensors based on dielectric resonators, such as ring resonator and photonic crystal cavities, as well as localized surface plasmon sensors [7, 14–26], since all these sensors are based upon shifting the resonant frequency of a single resonance. Below we refer to the limit of Eq. (3) as the *single-mode limit* for the spectral sensitivity in refractive index sensing. We will also refer to spectral sensitivity that is above the single-mode limit as *extraordinary.*

3. Extraordinary sensitivity in SPR sensors

The sensitivity in standard SPR sensors can easily reach 10^4 nm/RIU [10], which is well above the single-mode limit as described in the previous section. In this section, we will show that the SPR sensor achieves such an extraordinary sensitivity by employing multiple optical modes in the sensing scheme.

We again start with a specific example, by using a transfer matrix method to simulate a typical SPR sensor as shown in Fig. 1a. Here, for concreteness we assume a silver film of thickness 50nm. The dielectric constant of silver is modeled with a Drude model, with parameters from [33]. The prism has a refractive index n_{prism}=3.5. The medium above the silver is assumed to have n=1. The sensing region is the entire space above the silver. When the probing wave is incident from a fixed direction having an angle of incidence $\theta = 16.68°$ with respect to the prism-metal interface, a resonant dip is produced in the reflection spectrum at 1500nm wavelength (Fig. 1b, blue line). When the refractive index of the region above the silver film is increased by $\Delta n = 0.001$, the transmission dip shifts by 91nm (Fig. 1b, red line), corresponding to a spectral sensitivity $S = 91000$ nm/RIU. Such a sensitivity clearly exceeds the single-mode limit of 1500nm/RIU at this wavelength assuming n=1, and is therefore extraordinary.

The origin of such extraordinary sensitivity can be understood by analyzing the relevant dispersion relations. The dispersion relation of the probing wave inside the prism is

$$k_i = \frac{\sin(\theta)n_{prism}}{c}\omega \qquad (5)$$

where k_i is the wavevector component parallel to the top surface of the prism. The resonant dip in the reflection spectrum appears when the propagating wave inside the prism is phase-matched to the surface-plasmon waves at the metal-air interface:

$$k_i(\omega) = k_s(\omega, n) \qquad (6)$$

where k_s is the parallel wavevector of the surface plasmon. Here n is the refractive index of sensing region. n=1 for air in the example here. Such a phase-matching condition is illustrated in Fig. 3a.

When a small refractive-index perturbation Δn is introduced to the air region above the metal film, the dispersion relation of the surface plasmon shifts (red line in Fig. 3a). At a constant parallel wavevector k_s, the frequency shift $\Delta\Omega$ (Fig. 3a) of the surface plasmon mode can be calculated using the perturbation theory [32] and is subject to the same single-mode limit as described by Eq. (2). However, the shift $\Delta\omega$ in the resonance dip measured is much larger (Red dot in Fig. 3a). Since the position of resonance dip is determined by the phase matching condition, the resonance dip is now associated with a *different* surface plasmon mode at a *different* parallel wavevector. The key in the extraordinary sensitivity of SPR sensor lies in the presence of multiple modes (in this case, the entire surface plasmon dispersion relation representing a continuum of modes with different modes having different

wavevectors), and a specific design of the dispersion relation of the probing wave that exploits such a multi-mode nature.
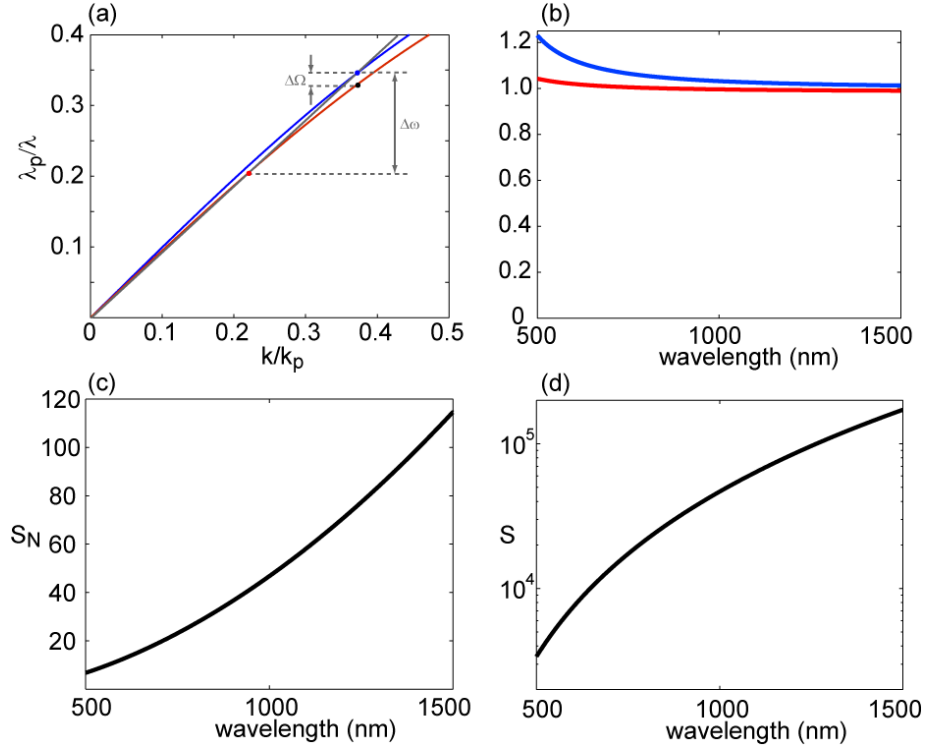

Fig. 3. Analysis of the SPR sensor. (a) Blue line is the dispersion relation for the surface plasmon mode at the metal-air interface. Red line represents the dispersion relation of the surface plasmon mode at the same interface when a small index perturbation is applied to the air region. Gray line is the dispersion relation of the propagation wave inside the prism. $k_p = \omega_p / c$ and $\lambda_p = 2\pi / k_p$, where ω_p is the plasmon frequency of the metal. (b) The group index (blue) and phase index (red) of the surface plasmon modes. In order to achieve a resonance at a given wavelength, the group index of the probe is chosen to match the phase index of the surface plasmon. (c) and (d) Normalized spectral sensitivity (c) and spectral sensitivity (d) as a function of operation wavelength for SPP sensor.

We now explicitly calculate the sensitivity using the phase-matching condition of Eq. (6). The solution to Eq. (6) determines the resonant wavelength λ. To see how the resonant wavelength changes with respect to refractive index perturbation, we take the derivative on both sides of Eq. (6) and obtain

$$\frac{d\omega}{dn} = \frac{\partial k_s / \partial n}{dk_i / d\omega - \partial k_s / \partial \omega} \tag{7}$$

Equation (7) can be used to determine wavelength sensitivity as

$$S = \frac{d\lambda}{dn} = -\frac{\lambda^2}{2\pi c}\frac{d\omega}{dn} = \frac{\lambda^2}{2\pi}\frac{\partial k_s}{\partial n}\frac{1}{n_g - n_{gi}} \tag{8}$$

where $n_g = \dfrac{c}{d\omega / dk_s}$ is the group index of the surface plasmon at λ, and

$$n_{gi} \equiv \frac{c}{\mathrm{d}\omega / \mathrm{d}k_i} = n_{prism} \sin\theta \qquad (9)$$

is the group index of the dispersion relation (Eq. (5)) for the probing wave inside the prism. Using the phase-matching condition of Eq. (6), we see that n_{gi} is the same as the phase index $n_p = ck_s / \omega$ of the surface plasmon at the resonant wavelength λ.

The factor $\dfrac{\lambda^2}{2\pi} \dfrac{\partial k_s}{\partial n}$ in Eq. (8) depends on the details of the dispersion, operation wavelength, and the overlap between the sensing region and the optical mode. In the SPR sensor, since the surface plasmon is confined at the metal-air interface, the strong overlap between the surface plasmon modes and the region with refractive index perturbation is indeed advantageous. Modal overlap argument alone, however, cannot explain the extraordinary sensitivity of the SPR sensor. Instead, as can be seen in Eq. (8), the sensitivity of a SPR sensor in fact diverges when the phase and group indices of the surface plasmon modes match, i.e. $n_g = n_p$.

In practice, using the phase-matching condition (Eq. (6)), one can choose to operate at different resonant wavelength λ by choosing an appropriate angle of incidence θ. Thus, we can plot the sensitivity of the SPR sensor as a function of resonant wavelength λ. As the resonant wavelength increases, the difference between the phase and group indices of the surface plasmon decreases (Fig. 3b). The normalized sensitivity is larger than 1 and increases with the wavelength (Fig. 3c). Figure 3d shows the sensitivity as a function of wavelength. The sensitivity of $10^4 - 10^5$ nm/RIU in the near infrared region significantly exceeds the single-mode limit, and is due entirely to the fact that the group and phase indices of surface plasmon nearly matches in this wavelength range.

As a conclusion of the analysis above, we emphasize the SPR sensor achieves extraordinary sensitivity with the use of multiple optical modes. *Before and after a refractive-index perturbation is applied to the sensing region, the transmission dips are produced by different surface plasmon modes having different parallel wavevectors.* Therefore, to draw contrast to the single-mode sensing scheme as described in Section 2, we refer to the SPR sensor as a *multi-mode* sensor. In such a multi-mode sensing scheme, even though the spectral shift of any single optical mode at a fixed parallel wavevector in the system is subject to the single-mode limit, the spectral sensitivity, which measures the spectral shift of the reflection dip, can be significantly larger. In contrast, in the Fabry-Perot dielectric sensor shown in Section 2, the resonance feature in the transmission spectrum is always associated with the same optical mode, and is therefore constraint by the single-mode limit.

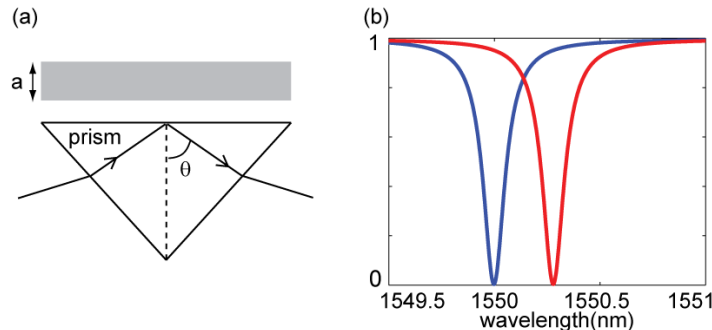## 4. Dielectric waveguide sensors with extraordinary sensitivity

Fig. 4. Dielectric waveguide sensor with extraordinary sensitivity. (a) Schematic of the sensor structure, consisting of a dielectric waveguide (gray region) separated from the top surface of the prism with an air gap. (b) Reflection spectra of the structure vary from the blue curve to the red curve, as an index perturbation $\Delta n = 10^{-5}$ is applied to the dielectric waveguide.

In the previous section we have illustrated the origin of extraordinary sensitivity in SPR sensor. In this section, we show that such extraordinary sensitivity is not unique for SPR, by designing dielectric waveguide sensors with similar sensitivity.

We consider a dielectric waveguide sensor structure as shown in Fig. 4a. The sensor structure consists of a lossy dielectric waveguide ($n = 1.5 + i10^{-6}$) with a thickness of 2000nm placed on top of a high-refractive index prism ($n=3.5$). There is a 1000nm thick air ($n=1$) gap between the waveguide and the prism. The probing light is incident from one side of the prism and the reflection is collected on the other side. The absorption loss in the waveguide results in a resonance dip in the reflection spectrum when the probe light phase-matches with the waveguide mode.

This class of waveguide sensor structure has been proposed and analyzed in Ref [1, 6]. However, the possibility of achieving extraordinary sensitivity in this system has not been recognized before. Here, we demonstrate extraordinary sensitivity by choosing the incident angle $\theta = 24.77^\circ$, which creates a resonant dip at wavelength 1550nm. When the refractive index of the waveguide are increased by $\Delta n = 10^{-5}$, the transmission dip red-shifts by 2.8nm, corresponding a sensitivity $S = 28000$ nm/RIU (Fig. 4b). The spectra are obtained by using a transfer matrix method to solve the Maxwell's equations. This is significantly larger than the single-mode limit of 1000nm/RIU at the same wavelength.
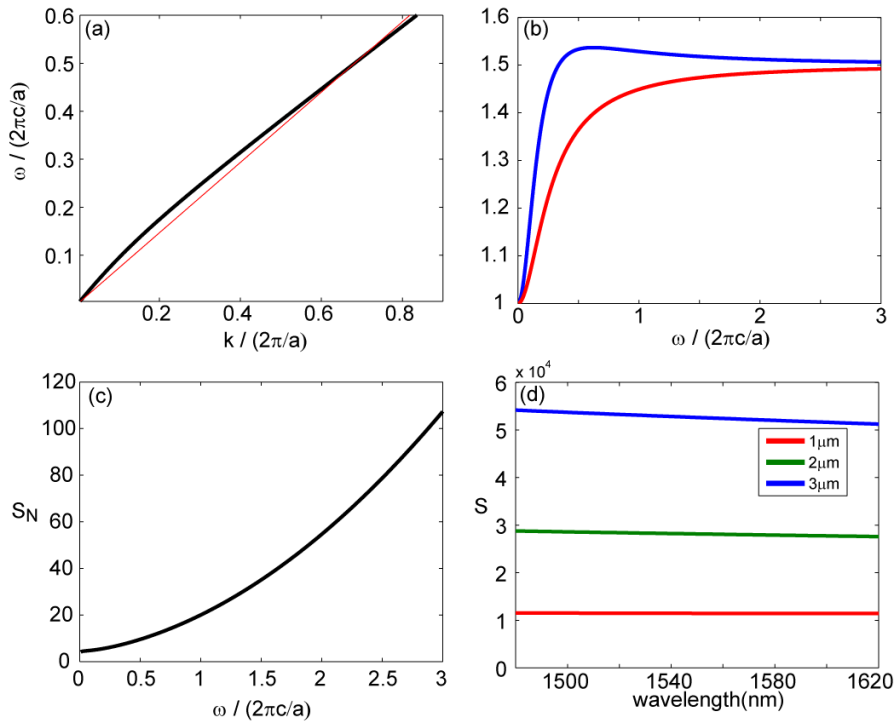

Fig. 5. (a) The black curve is the dispersion curve of the fundamental mode for a slab waveguide with a thickness of a and an index of $n=1.5$. The red curve is the dispersion curve of the probing light in the prism. (b) Group indices (blue line) and phase index (red line) of the dielectric waveguide. (c) Normalized spectral sensitivity for different operating frequency. (d) The spectral sensitivity for waveguides with different thicknesses.

For this class of sensors, the condition for achieving extraordinary sensitivity can be obtained using an analysis similar to the SPR sensors. In general, we consider the dielectric waveguide having a thickness a. A resonance is created when the dispersion relation of the probe light (red line in Fig. 5a) intersects with the waveguide dispersion relation (black line, Fig. 5a). The point of intersection in Fig. 5a defines the resonant wavelength λ. At the

resonant wavelength, the sensitivity of the structure can then calculated using Eq. (8), and diverges when the group and phase indices of the waveguide mode match.

In Fig. 5b, we plot the group and phase indices of the waveguide. These two indices approach each other in the regions of both high frequencies $(a/\lambda \gg 1)$ and low frequencies $(a/\lambda \ll 1)$ (Fig. 5b). Both these regions can provide extraordinary sensitivity. The calculated normalized spectral sensitivity of this structure is shown in Fig. 5c. The structure exhibits extraordinary sensitivity over wide ranges of operating frequencies.

In Fig. 5c, we notice that normalized sensitivity increases as a function of frequency. In our example here the sensing region is the dielectric region of the waveguide. At high frequency region, the waveguide modes are well confined to the dielectric layer, resulting in a good overlap between the optical modes and the sensing region, i.e. the dielectric layer. On the other hand, we expect the low frequency region, or equivalently, at a given operating frequency, a thinner waveguide, to be the optimal region of operation if instead the aim is to sense index changes in the air region above the waveguide. Extraordinary sensitivity can be accomplished in this low-frequency region as well.

Figure 5d shows the sensitivities calculated for three waveguides with different widths operating around 1550nm wavelength. The sensitivity increases with waveguide width. A wider waveguide corresponds to a higher normalized frequency in Fig. 5c and thus has a higher sensitivity. At the wavelength of 1550nm, for the thickness of the waveguide $a = 2$ μm, the analytic result in Fig. 5d is consistent with the numerical results in Fig. 4b.

To conclude this section, we note that, while both SPR sensor and the dielectric waveguide sensor here can achieve extraordinary sensitivity, the dielectric waveguide sensor here can have a lower loss and higher quality factor. The example in Fig. 5, where the assumed dielectric loss is in fact quite achievable with glass, possesses a quality factor of Q=12900, whereas the quality factor of a surface plasmon sensor is typically below 100. Here, the quality factor is obtained by measuring the ratio between the resonance wavelength and the full width at half maximum (FWHM) of the simulated spectrum. In comparing different sensors, it is in general more meaningful to compare their detection limits, defined as the minimum index shift that is detectable. The detection limit is related to the product of the quality factor and the spectral sensitivity [27]. Thus, the dielectric waveguide sensor structure as proposed here, which combines extraordinary spectral sensitivity with high quality factor, should allow for significant lower detection limit compared with the SPR sensor and therefore should possess a fundamental advantage in terms of its optical performance over the SPR sensors.

5. Enhancing spectral sensitivity by manipulating the probe dispersion relation

In this section, we show that the sensitivity of both the SPR and the waveguide sensors can be further enhanced if we allow the angle of incidence to vary as well during the spectral measurement process. The key idea here is to design the dispersion relation of the probe to better match the dispersion relation of either the surface plasmon modes or the waveguide modes.

The concept of designing the dispersion relation of the probe can be seen by examining Eq. (8), which has been used to calculate the sensitivity for both the SPR sensor and the waveguide sensors in the previous two sections. In previous sections, we have assumed a constant incident angle θ. The dispersion relation of the probe wave is then

$$k = n_{prism} \sin(\theta) \frac{\omega}{c} \equiv n_{gi} \frac{\omega}{c} \qquad (10)$$

The key for high sensitivity has been the approximate matching of the group index n_{gi} of the probe to the group index n_g of the surface plasmon or the waveguide mode. Such a matching can be done more effectively by designing a probing scheme as described by the dispersion relation

$$k - k_0 = n_d(\omega - \omega_0)/c \qquad (11)$$

where (k_0, ω_0) is the wavevector and the frequency of the resonance. By definition, the resonance (k_0, ω_0) lies on the dispersion relation curve of the waveguide mode. n_d is the designed group index of the probe wave. The sensitivity of the sensing scheme should then be enhanced when n_d is chosen to match n_g. Figure 6a shows two different probes with group indices 0.75 and 1. The black curves represent the dispersion of the waveguide mode without (solid line) and with (dashed line) an index perturbation. The dispersion curves are approximately linear within the small frequency range considered here. The observed frequency shift Ω_2, for the larger probe index $n_d=1$ (green line), is indeed larger than Ω_1 as observed with a probe index $n_d=0.75$ (blue line). The sensitivity is therefore improved as n_d approaches n_g.
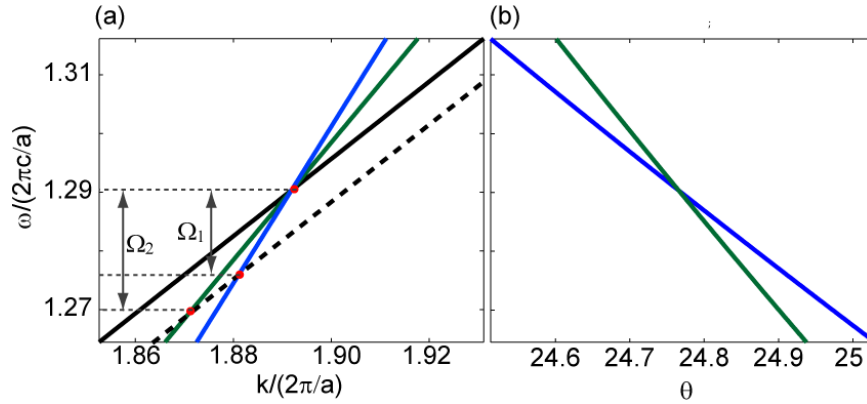

Fig. 6. (a) Design of the dispersion relation of the probes. The black solid and dashed curves correspond to the waveguide dispersion relations without or with index perturbations, respectively. The blue and green curves are the dispersion relations for the probe waves, having different group indices $n_d=1$ (green curve), and $n_d=0.75$(blue), respectively. (b) Incident angle as a function of incident light frequency for the two different probe waves shown in (a).

Such a probe dispersion relation can be achieved by varying angle of incidence as a function of frequency

$$\theta(\omega) = \arcsin\left(\frac{n_d(\omega - \omega_0) + ck_0}{n_{prism}\omega} \right) \qquad (12)$$

Figure 6b shows the required frequency dependency for the incident angle. Different probe indices require different functions of $\theta(\omega)$. By varying the angle of incidence according to Eq. (12), one can create dispersion curves with any probe index n_d.

We now numerically demonstrate the enhancement of sensitivity through the control of the group index of the probe, by again considering the same system as in Fig. 4a, where the sensing region consists of a 2000nm thick waveguide ($n = 1.5 + i10^{-6}$) and the operating wavelength is in the vicinity of 1550nm. In Section 4, we have shown that this structure, when probed with waves at a constant angle of $\theta_0 = 24.77°$, exhibits a resonant dip at wavelength $\lambda_0 = 1550$nm, with a spectral sensitivity of $S = 2.8 \times 10^4$ nm/RIU. Such a constant-angle probe wave has a dispersion relation of the form of Eq. (11), with $n_d = n_{prism} \sin(\theta_0) = 1.466$, as discussed in Section 4. Here, instead of a constant-angle probe wave, we use a different probe wave with a dispersion relation of Eq. (11). Here, the same values of ω_0, k_0 as described above are used, but we vary n_d between 0.75 and 1.5. We

numerically simulate the reflection spectra with the same setup as that in Fig. 4a. Due to the choice of the values of ω_0, k_0, for each choice of n_d here, in the absence of index perturbation in the waveguide, the resonant peak is at 1550nm. When we apply a refractive index perturbation $\Delta n = 10^{-5}$ to the waveguide, the resonant wavelength shifts. The spectral sensitivity varies significantly as n_d varies. The sensitivity increases dramatically when the probe index approaches the waveguide group index at 1.52. As n_d increases from 0.75 to 1.45 to 1.5, the sensitivity increases from 2×10^3 nm/RIU to 2×10^4 nm/RIU to 7×10^4 nm/RIU (Figs. 7b-d). The numerical simulations are consistent with the analytical results shown in Fig. 7a. Thus, we have shown that in this class of multi-mode spectral sensor, there is in fact no upper limit of spectral sensitivity. Instead, by a choice of an appropriate probe wave that has a dispersion relation matching that of the waveguide mode, arbitrarily high spectral sensitivity can in principle be achieved.
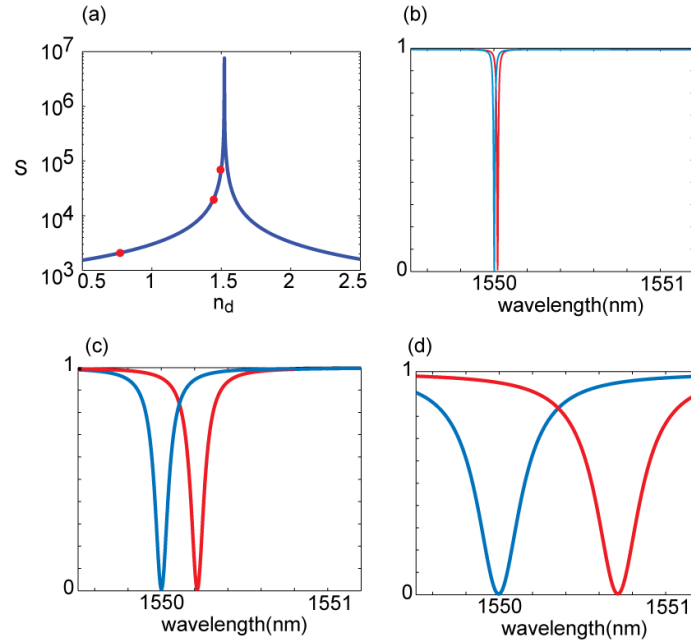

Fig. 7. (a) Spectral sensitivity for different probe indices. Red dots are from numerical simulations. (b-d) The shift of reflection spectra with different probe indices: n_d =0.75 (b), n_d =1.45(c), and n_d = 1.5(d).

In Fig. 7b-d, we also note that the quality factor of the resonance dip decreases when the sensitivity increases. This is in fact a general observation for this class of multi-mode sensors considered here. The waveguide modes at a given parallel wavevector k have a finite lifetime due to the waveguide loss and the radiative leakage through the prism. The inverse of such a lifetime corresponds to the linewidth $\Delta\omega$ for the waveguide mode. For the probe with the dispersion relation as shown in Eq. (11), the reflection spectrum has a resonance with a linewidth

$$\Delta\Omega = \frac{n_g}{n_g - n_d} \Delta\omega \qquad (13)$$

as can be seen geometrically by examining Fig. 8a. Similar to the behavior of the spectral sensitivity, the linewidth of the resonance spectrum also increases as the group index of the probe n_d approaches the group index of the waveguide mode n_g

Defining a quality factor for the sensor $Q = \omega / \Delta\Omega$, and combining Eq. (8) with (13), we obtain a general constraint:

$$SQ = \frac{\lambda}{\Delta\omega} \frac{\partial k_s}{\partial n} \frac{1}{n_g} \qquad (14)$$

The product of Q and sensitivity S is thus independent of the dispersion relation of the probe. Figure 8b plots the simulations results (red dots) of the quality factors and sensitivity for different probes in the structure used in Fig. 7, where we vary n_d from 1.52 to 0.75. The linear relation in this logarithmic plot agrees with Eq. (14).
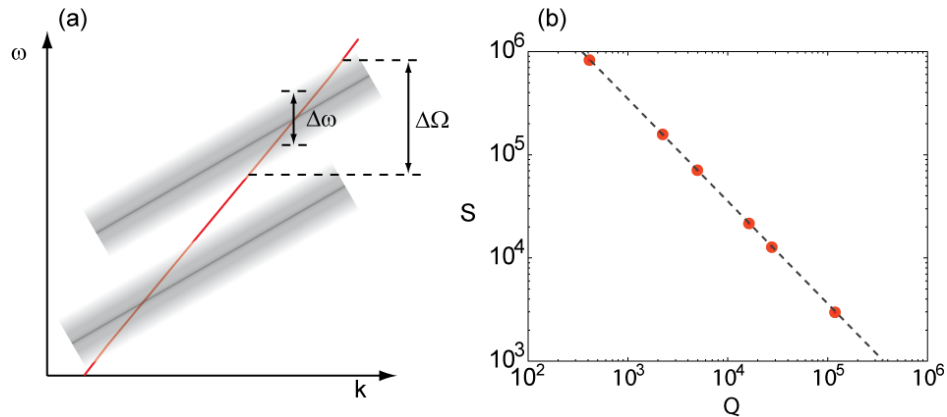

Fig. 8. (a) The dispersion diagram showing the width of waveguide resonance $\Delta\omega$ and the apparent width $\Delta\Omega$ in the reflection spectra. The upper (lower) grey line is the dispersion curve of the waveguide mode without (with) an index perturbation, respectively. The red line represents the dispersion curve of the probe light. (d) The relation between the sensitivity and quality factor for the same sensor structure shown in Fig. 4a, but with different probe indices. Red dots are from simulation and they follow a linear relation in the logarithm plot.

Since the detection limit of a sensing scheme is in general determined by the product between the quality factor and the spectral sensitivity, the relation of Eq. (14) shows that designing different probe could not improve the detection limit. In order to improve the detection limit, one needs to reduce the intrinsic bandwidth of the photonic states $\Delta\omega$, for example by using low-loss photonic structures. However, understanding the tradeoff between the sensitivity and quality factor could be practically useful. For instance, large spectral sensitivity relaxes the resolution requirement of the spectrometers and the wavelength stability of the laser used in the sensing schemes.

6. Conclusion

We show that the origin of the extraordinary spectral sensitivity of SPR sensor is the use of multiple optical modes. Such multi-mode sensing scheme can also be implemented in dielectric sensors to achieve extraordinary spectral sensitivity. In principle, one can design the dispersion relation of the probing wave to achieve arbitrarily-large spectral sensitivity. We also point out an inherent tradeoff between the linewidth and the spectral sensitivity in such multi-mode sensing schemes. The intrinsic tradeoff between the quality factor and the spectral sensitivity shows that the detection limit of a resonance-sensing scheme is ultimately determined by the intrinsic bandwidth of the resonances supported by the system.

Acknowledgement